Tellus (2001), 53A, 245–265
Printed in UK. All rights reserved

TELLUS
ISSN 0280–6495

Polynyas in a high-resolution dynamic–thermodynamic sea ice model and their parameterization using flux models

By H. BJORNSSON[1], A. J. WILLMOTT[2]*, L. A. MYSAK[3] and M. A. MORALES MAQUEDA[4], [1]*Program in Atmospheric and Ocean Sciences, GFDL, Princeton University, New Jersey, USA;* [2]*Department of Mathematics, Keele University, Staffordshire ST5 5BG, UK;* [3]*Department of Atmospheric and Oceanic Sciences and Centre for Climate and Global Change, McGill University, Montreal, QC H3A 2K6, Canada;* [4]*Potsdam Institute for Climate Impact Research, PO Box 60 12 03 14412 Potsdam, Germany*

(Manuscript received 6 July 1999; in final form 3 September 2000)

ABSTRACT

This paper presents an analysis of the solutions for a steady state latent heat polynya generated by an applied wind stress acting over a semi-enclosed channel using: (a) a dynamic–thermodynamic sea ice model, and (b) a steady state flux model. We examine what processes in the sea ice model are responsible for the maintenance of the polynya and how sensitive the results are to the choice of rheological parameters. We find that when the ice is driven onshore by an applied wind stress, a consolidated ice pack forms downwind of a zone of strong convergence in the ice velocities. The build-up of internal stresses within the consolidated ice pack becomes a crucial factor in the formation of this zone and results in a distinct polynya edge. Furthermore, within the ice pack the across-channel ice velocity varies with the across-channel distance. It is demonstrated that provided this velocity is well represented, the steady state polynya flux model solutions are in close agreement with those of the sea ice model. Experiments with the sea ice model also show that the polynya shape and area are insensitive to (a) the sea ice rheology; (b) the imposition of either free- slip or no-slip boundary conditions. These findings are used in the development of a simplified model of the consolidated ice pack dynamics, the output of which is then compared with the sea ice model results. Finally, we discuss the relevance of this study for the modelling of the North Water Polynya in northern Baffin Bay.

1. Introduction

Coastal polynyas in the Arctic and Antarctic contribute to the annual production of sea ice and to deep water formation. For example, in the Arctic, Aagaard et al Aagard et al. (1981) and Cavalieri and Martin (1994) suggest that the halocline could be maintained by sea ice growth over the continental shelves of the Arctic Ocean. A significant fraction of the sea ice production occurs within Arctic polynyas. In fact, Winsor and Björk (2000) estimate a mean ice production from all Arctic polynyas of $0.29 \pm 0.03 \times 10\ \mathrm{km}^3\ \mathrm{yr}^{-1}$ The saltflux resulting from this is about 30% of the estimated flux that is needed to maintain the Arctic halocline. Winsor and Björk identify the Barents, Kara, Chukchi and Bering Seas as important regions for contributing to halocline water formation, while the Chukchi Sea is the only area contributing to deep water formation. The production of deep water within coastal polynyas also occurs in the marginal seas of Antarctica (Grumbine, 1991). Deep water production within a polynya can results when negative buoyancy fluxes (due to brine rejection and surface heat loss to the atmosphere) become large enough to trigger convective overturning (Chapman and

* Corresponding author.
email: a.j.willmott@maths.keele.ac.uk

Gawarkiewicz (1997), Chapman (1999)) which mixes the dense surface water downward. If mixing occurs over the entire water column, a dense saline cold-water downslope current is created.

Theoretical understanding of wind driven polynyas is mainly based on "flux polynya models". In such models, the first of which proposed by Lebedev (1968), consolidated ice is driven by the wind away from the shore and is replaced by the near-shore formation of frazil ice. The balance of these two processes then governs the location of the polynya edge, and hence, the polynya's size. Based on this flux balance principle, Pease (1987) introduced a simple one-dimensional time-dependent model of a wind-driven polynya. This model has been extended in various ways, first by Ou (1988) to include finite drift rate of frazil ice and then by Darby et al. (1994), Darby et al. (1995), Willmott et al. (1997; hereafter referred to as WMMD). The latter three papers developed the steady state theory for a two-dimensional wind driven polynya with a specified ocean velocity field and free-drift momentum balance for the frazil ice. Finally, a time dependent version of the theory was developed by Morales-Maqueda and Willmott (2000, hereafter referred to as MMW).

An alternative to the flux theory is to use a numerical sea ice model to study polynyas. The comprehensiveness of a numerical sea ice model gives it some advantages over flux models. For example, a numerical model will allow for a dynamical treatment of the consolidated ice motion, something that is prescribed in flux models. Furthermore, various thermodynamic processes are explicitly treated in most sea ice models, whereas in flux models these enter through the ice production rate which is often prescribed as uniform in the polynya and neglected in the ice pack. Finally, numerical sea ice models are often one component of a coupled climate model, in which case it is possible to examine the effects of a polynya on the other model components (atmosphere or ocean). However, the present generation of global ocean circulation models (OGCMs) and climate models do not have small enough horizontal grid resolution to resolve all but the very largest coastal polynyas. One of the few global OGCMs which has been used to address the formation and maintenance of a coastal polynya, namely the Ross Sea Polynya, is due to Fichefet and Goose (1999). On a regional scale, Lynch et al. (1997) employed a high resolution (7×7 km grid) coupled atmosphere-sea ice model to simulate a polynya opening event in the St Lawrence Island, in the Bering Sea.

In this paper we apply a high resolution dynamic–thermodynamic sea ice model to investigate polynya formation and maintenance in fjords and bays. A semi-enclosed rectangular channel is used as a prototype fjord or bay in this study. As a main goal, we want to gain an understanding of what processes control the maintenance and shape of a polynya in such a sea ice model. In particular, this includes obtaining a simple dynamic description of the flow of the consolidated ice pack. A secondary goal of this paper is to examine to what extent the polynya in the sea ice model can be reproduced by a much simpler flux model. Finally, as a third goal, we want to see if it is possible to combine the two models, using simplified dynamics for the consolidated ice pack together with a polynya flux model, to describe both the polynya and the pack ice flow.

Two key results emerge from the study. The existence of a sharp polynya edge in fjords or bays depends on (i) the presence of land or an ice bridge in the upwind direction which favours ice divergence, and (ii) convergence and shearing of ice against the lateral boundaries of the bay creates a sea ice velocity discontinuity. Perhaps the most well known polynya in a bay is the North Water Polynya (NOW) located in northern Baffin Bay. Each year an ice bridge forms, blocking the southward drift of sea ice from the Arctic Ocean through Nares Strait into Baffin Bay. Frazil ice formed within the polynya drifts southward under the action of wind and currents to accumulate at the edge of the consolidated ice pack that often covers the entire width of the bay.

The plan of this paper is as follows. Section 2 presents the salient features of the steady state two-dimensional flux polynya model and the numerical sea ice model. In Section 3, steady state polynya solutions in a semi-enclosed channel are obtained for a variety of wind stress orientations using the sea ice model, and the results are then reconstructed making use of the flux theory. In Section 4, we examine in detail the sensitivity of the sea ice model polynya solutions to certain parameters in the sea ice rheology and boundary conditions. In Section 5, we present a theory that allows us to calculate the necessary parameters for the flux model, and we then compare the results of the combined model with the results of the ice model. The conclusions and discussions are given in Section 6.

2. The models

The two models used in this study are a recently developed sea–ice model and a simple polynya flux model. The former is a full dynamic–thermodynamic sea ice model developed by Tremblay and Mysak (1997; herafter referred to as TM), which is based on a granular material rheology combined with a zero-layer Semtner (1976) thermodynamic model. For a complete description of the polynya flux model, see MMW. Short descriptions of these models are given below.

2.1. *The flux model*

Polynya flux models have their origin in the idea that the balance between the flux of frazil ice produced within the polynya and the wind-driven divergence of ice from the coast determines the location of the steady state polynya edge, and hence the polynya's extent (Fig. 1). The polynya edge defined by this flux balance separates a region of nearly open water (the polynya) from a region

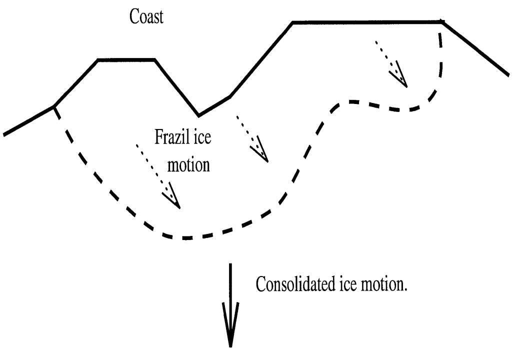

Fig. 1. A schematic picture of a wind driven polynya. Offshore winds drive the ice pack away from the coast (thick solid line), opening up a polynya. Frazil ice is formed within the polynya, and drifts towards the ice pack where it consolidates and forms the polynya edge (dashed line). The motion of the consolidated ice is shown as a solid arrow, and the frazil ice drift is shown as a set of dotted arrows.

with a discontinuous mat of consolidated new ice which has been formed by accretion of frazil ice arriving from the polynya. We shall refer to this latter region as the "consolidated ice region".

In this paper, we investigate steady state polynya solutions within a semi-enclosed channel. We assume that the frazil ice production rate, F, within the polynya is uniform. Let $\boldsymbol{u}$ and $\boldsymbol{U}$ denote the prescribed constant frazil ice velocity and consolidated ice velocity, respectively. Following MMW, let $C(\boldsymbol{r}) = \text{constant}$ denote the polynya edge, where $\boldsymbol{r}$ is the position vector of any point on the edge. At any point on C we have

$$\mathrm{d}\boldsymbol{r} \cdot \nabla C = 0. \tag{1}$$

MMW generalise the one-dimensional theory of Ou (1988) by demanding that the normal fluxes of frazil and consolidated ice across C balance. In other words

$$(H\boldsymbol{U} - h_{\mathrm{C}}\boldsymbol{u}) \cdot \nabla C = 0, \tag{2}$$

where H is the thickness of the consolidated ice at the edge and h_{C} the frazil ice depth arriving at C. Combining (1) and (2), the steady-state polynya edge satisfies the equation

$$\frac{\mathrm{d}y}{\mathrm{d}x} = \frac{HV - h_{\mathrm{C}}v}{HU - h_{\mathrm{C}}u}, \tag{3}$$

where $\boldsymbol{U} = (U, V)$ and $\boldsymbol{u} = (u, v)$.

Now consider a semi-enclosed channel of uniform width L. With respect to a right-handed Cartesian coordinate frame Oxyz, the vertical walls of the channel are located at $y = 0$, L and the end wall of the channel coincides with $x = 0$. If $\boldsymbol{u}$ is known over the entire polynya domain, h_{C} can be determined from the conservation equation of frazil ice mass, namely

$$\nabla \cdot (h\boldsymbol{u}) = F. \tag{4}$$

When $\boldsymbol{u}$ is constant, (4) reduces to

$$\boldsymbol{u} \cdot \nabla h = F. \tag{5}$$

Thus, along frazil ice trajectories, which are characteristic curves of (5),

$$\frac{\mathrm{d}h}{\mathrm{d}t} = F, \tag{6}$$

where t is the travel time from the coast to any point on a characteristic. On the coast, we demand $h = 0$, and therefore

$$h_{\mathrm{C}} = FT, \tag{7}$$

where T is the transit time along a characteristic from the coast to the polynya edge.

A key quantity of flux model theory is the *Lebedev–Pease width* of a polynya (Willmott et al., 1997). It is the width needed to balance the flux of consolidated ice (HU) given the ice production rate (F) and is given by

$$L_{\mathrm{p}} = \frac{HU}{F}. \tag{8}$$

To summarize, the steady state flux model which is used in this study is described by (3) and (7), in which H has a given value and $\boldsymbol{u}$, $\boldsymbol{U}$, and F are prescribed functions of $\boldsymbol{r}$. Given a point on the polynya edge, (3) can be numerically integrated (see WMMD for details), provided h_{C} can be determined. The latter field is found by numerically integrating (6) along the frazil ice trajectories subject to $h = 0$ on all coastal boundaries.

2.2. *The dynamic–thermodynamic sea ice model*

For large-scale simulations of the sea ice cover using slowly varying wind forcing, the inertia of sea ice can be neglected in the momentum balance equation. Under this approximation, the large-scale two-dimensional horizontal motion of sea ice can be described by

$$0 = -\rho_{\mathrm{ice}} hf\boldsymbol{k} \times \boldsymbol{u}_i + \tau_{\mathrm{a}} - \tau_{\mathrm{w}} + \nabla \cdot \boldsymbol{\sigma} - \rho_{\mathrm{ice}} hg \nabla H_{\mathrm{d}}, \tag{9}$$

where ρ_{ice} is the ice density, h the mean ice thickness, f the Coriolis parameter, $\boldsymbol{k}$ a unit vector normal to the ice surface, $\boldsymbol{u}_i$ the ice velocity, $\boldsymbol{\tau}_{\mathrm{a}}$ the wind stress on the top ice surface, $\boldsymbol{\tau}_{\mathrm{w}}$ the ocean drag, $\boldsymbol{\sigma}$ the vertically integrated internal ice stress tensor, g the gravitational acceleration, and ∇H_{d} the slope of the sea-surface.

The air and water stresses are obtained from simple linear drag laws. In this model the sea ice is assumed to behave as a granular material in slow continuous deformation. The resistance to compressive load is a function of its thickness and concentration, and its shear resistance is proportional to the internal ice pressure at a point. In divergent motion, the ice offers no shear resistance, and the floes drift freely.

The distribution of ice is characterized by both the mean ice thickness h and ice concentration A (% of a grid cell covered by ice). The conservation of both quantities is given by

$$\frac{\partial h}{\partial t} + \nabla \cdot (h\boldsymbol{u}_i) = S_{\mathrm{h}}, \tag{10}$$

$$\frac{\partial A}{\partial t} + \nabla \cdot (A\boldsymbol{u}_i) = S_{\mathrm{A}}, \tag{11}$$

where S_{h} and S_{A} are the thermodynamic source terms, which take the form

$$S_{\mathrm{h}} = \frac{1}{\rho_{\mathrm{ice}} L_{\mathrm{f}}} \begin{cases} A(Q_{\mathrm{ia}} - Q_{\mathrm{oi}}) + (1-A)Q_{\mathrm{oa}}, & T_{\mathrm{o}} = T_{\mathrm{of}},\ Q_{\mathrm{oa}} > 0 \\ A(Q_{\mathrm{ia}} - Q_{\mathrm{oi}}), & T_{\mathrm{o}} > T_{\mathrm{of}} \end{cases} \tag{12}$$

$$S_{\mathrm{A}} = \frac{1}{\rho_{\mathrm{ice}} L_{\mathrm{f}}} \begin{cases} (1-A)Q_{\mathrm{oa}}/h_0, & T_{\mathrm{o}} = T_{\mathrm{of}},\ Q_{\mathrm{oa}} > 0 \\ A\rho_{\mathrm{ice}} L_{\mathrm{f}} S_{\mathrm{h}}/2h, & S_{\mathrm{h}} < 0. \end{cases} \tag{13}$$

In (12) and (13), L_{f} is the latent heat of fusion, Q_{ia} and Q_{oa} are the net ice and oceanic heat fluxes to the atmosphere, Q_{oi} is the ocean–ice sensible heat flux, h_0 is a fixed demarcation thickness between thin and thick ice (Hibler, 1979), and T_{o} and T_{of} are respectively the temperature and freezing point temperature of the ocean.

The ice–atmosphere heat flux is the net heat flux due to longwave (up and down) radiation, shortwave radiation, sensible heating and latent heating, and can be written as (all fluxes are measured positive upwards)

$$\begin{aligned} Q_{\mathrm{ia}} = {} & \varepsilon_{\mathrm{i}} \sigma T_{\mathrm{i}}^4 - \varepsilon_{\mathrm{a}} \sigma T_{\mathrm{a}}^4 - Q_{\mathrm{sw}}(1-\alpha_{\mathrm{i}}) \\ & + \rho_{\mathrm{a}} C_{\mathrm{sens}} |\boldsymbol{u}_{\mathrm{a}}| C_{\mathrm{pa}} (T_{\mathrm{i}} - T_{\mathrm{a}}) \\ & + \rho_{\mathrm{a}} C_{\mathrm{lat}} |\boldsymbol{u}_{\mathrm{a}}| L_{\mathrm{s}} (q_{\mathrm{i}} - q_{\mathrm{a}}), \end{aligned} \tag{14}$$

where ε_{i} and ε_{a} are, respectively, the emissivities of the ice and the atmosphere, σ the Stefan–Boltzmann constant, T_{i} and T_{a} are respectively the ice surface temperature and the air temperature, Q_{sw} the daily averaged flux of solar radiation at the surface, α_{i} the ice albedo, ρ_{a} the air density, $|\boldsymbol{u}_{\mathrm{a}}|$ the wind speed, C_{sens} and C_{lat} the sensible and latent heat transfer coefficients respectively, C_{pa} the specific heat of air, L_{s} the latent heat of sublimation, and q_{i} and q_{a} the ice surface (assumed saturated) and atmospheric specific humidities (assumed to be at 80% of saturation). The saturation vapour pressure used to calculate the humidities is found from standard formulas (Rogers and

Yau, 1989). Similar expressions are used for the ocean–atmosphere and ice–ocean heat transfers.

For thin ice and slowly varying air temperature the time dependent terms in the ice energy equation can be neglected and the resulting equation for the ice temperature $[T_{\mathrm{ice}}(z)]$ assumes the form

$$K_{\mathrm{i}} \frac{\partial^2 T_{\mathrm{ice}}}{\partial z^2} = 0, \tag{15}$$

where K_{i} the ice thermal conductivity.

Further details on the sea ice model and its numerical scheme can be found in TM.

3. Model experiments

The model domain chosen for illustrating the results is a 50 km-wide and 100 km long channel (Fig. 2). The gridsize used is 2 km, and the timestep 1/200 of a day. The channel is open at one end, and sea ice is allowed to drift freely out. To ensure that this open boundary did not affect the solution at 100 km, we performed the calculations for a 115 km long channel.

The ice model is initialized with 20 cm thick ice and 90% concentration. Air temperature is prescribed at $-10°$C and kept constant. The ocean-surface temperature is held at the freezing point ($-1.8°$C), and no ocean currents are prescribed. The ocean surface is assumed to be flat, so the slope term in (9) is zero. The shortwave radiation is calculated according to Zillman (1972). An average of $Q_{\mathrm{sw}} = 35$ W/m^2 is found to be representative for the high-latitude early spring time solar radiation. In the following model runs, for simplicity, the Coriolis force is neglected.

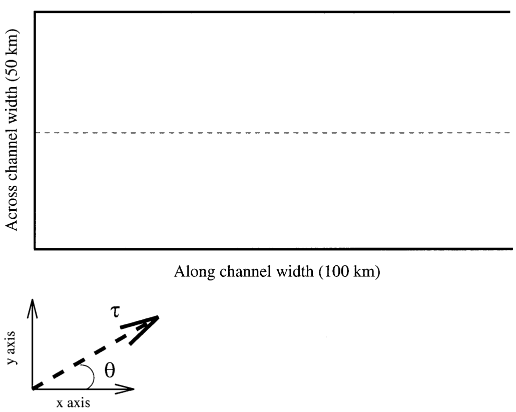

Fig. 2. The model domain. The width of the channel is 50 km. Also shown are the x and y axis and the wind-stress $\boldsymbol{\tau}$. The various experiments use different wind direction (θ). The dashed line in the middle of the domain shows the location of the transect used in Fig. 3.

When ice forms in a model grid cell in which $A < 1$, an assumption must be made about the thickness of the newly formed ice, so that the concentration can be updated. This value is set by the demarcation thickness h_0 in (13) and controls the thickness at which the newly formed ice collects. When modelling the large-scale Arctic ice cover, a value of $h_0 \simeq 1$ m is chosen so that the resulting ice cover exhibits a realistic seasonal cycle (see TM for details). For a polynya, where the ice thickness is generally lower, this value h_0 is too high. If the wind is strong enough in a region where frazil ice is forming, Langmuir circulation will collect the frazil into rows, resulting in frazil ice streaks and leaving the rest of the water free to form more ice (Pease, 1987; Smith et al., 1990). For the Odden Ice tongue in the Greenland Sea there is observational evidence (Brandon and Wadhams, 1999a) supported by modelling results (Kampf and Backhaus, 1999) to indicate that the frazil in the streaks stays in suspension within a few meters of the surface. However, using a collection thickness value of a few meters is not realistic, since the frazil ice in the streaks is a loose collection of ice crystals suspended in the water column, and if this collection was compacted, the total thickness of the compacted ice would be much lower. Indeed, frazil ice is often transformed into compacted "pancake ice" through interaction with the oceanic wave field. The latter ice type is more compact and thinner, with a typical thickness on the order of 10 cm (Brandon and Wadhams, 1999b), a value which should be regarded as an absolute lower bound on h_0. In view of this we set $h_0 = 30$ cm, which leads to reasonable ice concentrations (i.e., $A < 50\%$) within the polynya, where the ice formation rate is highest. The values of the physical parameters used in the sea ice model are given in Table 1.

3.1. *Along-channel winds* ($\theta = 0$)

In the first set of experiments, a uniform wind (of 20 m/s) was directed down the channel. At first, we ran the TM model with thermodynamics

Table 1. *Main physical parameters and constants used in the simulation*

Variable	Symbol	Value
ice albedo	α_i	0.70
atmospheric emissivity	ε_a	0.88
ice emissivity	ε_i	0.97
air density	ρ_a	1.3 kg/m^3
ice density	ρ_{ice}	900 kg/m^3
ocean density	ρ_w	1000 kg/m^3
air and water turning angle	θ_a, θ_w	0°
ice strength parameters	C, P^*	30, 5×10^3 N/m^2
angle of dilatancy	δ	0°
internal angle of friction	ϕ	30°
air drag coefficient	C_{da}	5×10^{-3}
water drag coefficient	C_{dw}	5×10^{-4}
latent heat transfer coefficient	C_{lat}	1×10^{-3}
specific heat of air	C_{pa}	1×10^3 J/(jg K)
specific heat of ice	C_{pi}	2×10^3 J/(kg K)
sensible heat coefficient	C_{sens}	1×10^{-3}
ice thermal conductivity	K_i	2 W/(m^2 K)
latent heat of fusion	L_f	3.30×10^5 J/kg
latent heat of sublimation	L_s	2.83×10^6 J/kg
net insolation to surface	Q_{sw}	35 W/m^2
ocean freezing point	T_{fp}	-1.8°C
coriolis parameter	f	0 s^{-1}
ice demarcation thickness	h_0	0.3 m

absent, and then repeated the run with the thermodynamics included. In both cases the model was integrated for 50 model days. Fig. 3 shows the ice thickness and concentration fields obtained both with and without the thermodynamic ice model for the first 5 days of the integration. These results highlight the fact that due to ice freezing, steady state ice cover is reached when thermodynamics are included.

Fig. 3 shows the time evolution of the ice thickness and concentration on a transect at $y = 25$ km, (i.e., the axis of the channel shown as a dashed line in Fig. 2). In the absence of thermodynamic ice growth, we would expect to see the ice drift out of the domain, leaving open water in its wake. This is indeed what is observed in Figs. 3b, d. In contrast, when thermodynamics is introduced (Figs. 3a, c) ice formation within the polynya balances the export of ice out of the domain after approximately 4 days resulting in a steady state ice cover. Notice that the steady state for ice thickness (Fig. 3a) is first reached for the thin ice· the 0.1 m thick ice has reached equilibrium after 1.5 days (after this day the 0.1 m contour-line is vertical), but 0.25 m thick ice takes about 4 days to reach equilibrium. For the ice concentration (Fig. 3c) the situation is similar. The lower concentrations (in the range 0.1–0.5) spin-up within three days however the higher concentrations take longer to spin-up.

Fig. 4 shows the ice thickness, ice drift velocity, ice concentration and ice flux divergence after 50 days of integration. Inspection of Fig. 4 shows, however, that while a steady state ice cover is reached, a polynya with a clearly identifiable polynya edge does not form. With flux models, there is no ambiguity in where the polynya edge lies. Both the thickness and velocity of the consolidated ice are specified, and hence the mass flux of consolidated ice is known. The edge of the polynya is then located where the frazil and consolidated ice fluxes normal to the edge are in balance. The lack of a clear polynya edge in the sea ice model is not due to a failure to achieve this ice flux balance, since that balance holds throughout the sea ice model domain (as a consequence of (10)). Rather, it is associated with the fact that the along-channel ice velocity is everywhere in free-drift, and as a consequence we do not obtain two distinct velocity fields associated with frazil and consolidated ice, as postulated in flux models.

To generate a polynya edge in the ice model, one can introduce inhomogeneities in the ice velocity field, and force ice convergence (i.e., either retard the consolidated ice motion or accelerate the thin (frazil) ice). In Subsection 3.2 below we discuss cases where an on-shore wind results in the build-up of internal stresses in the consolidated ice, which slows down its motion. In the absence of such internal stresses, the possibility of accelerated frazil ice drift can occur in nature through Stokes drift in the open waters of the polynya, or through an enhanced downwind surface current in the Langmuir surface convergence lines where the frazil ice collects (Smith et al., 1990).

A straightforward way to parameterize this latter effect in a sea ice model is to modify the drag law, so that when ice concentration is high, the air–ice drag has the control value, but when the ice concentration is low, there is enhanced air–ice drag, resulting in greater speeds of thin ice. To test this we ran a case where the air–ice drag coefficient (C_d) was a function of the ice concentration. We used $C_d(A) = C_d^{ctrl} \times \mathscr{F}(A)$ where

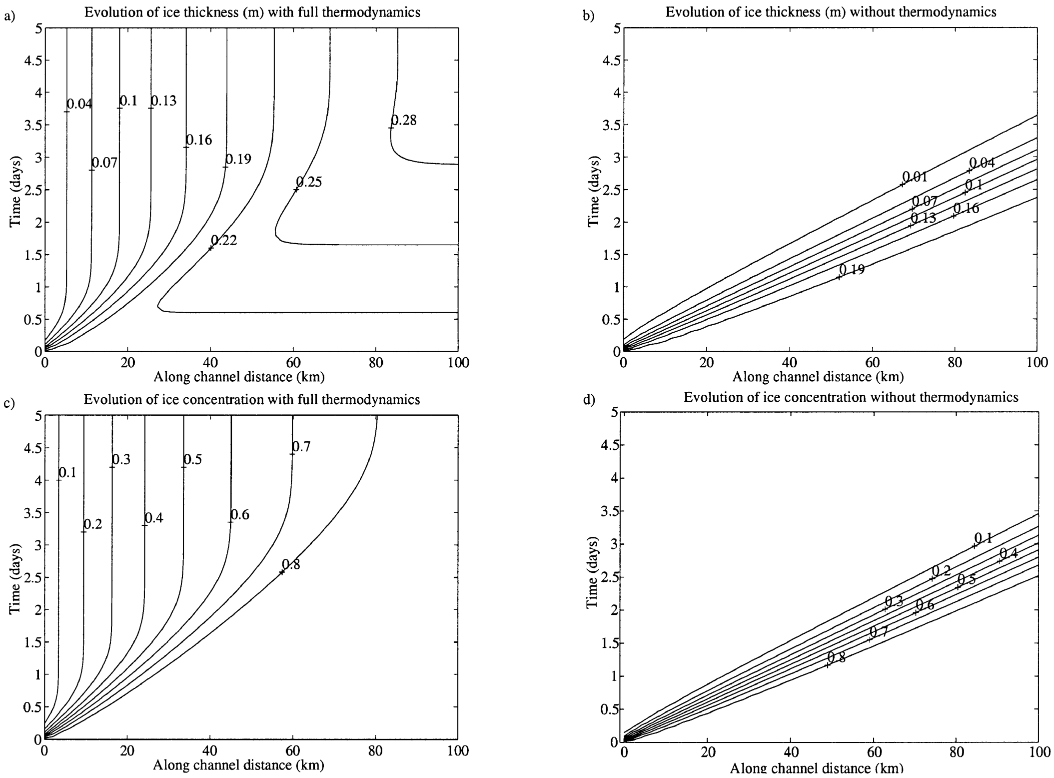

Fig. 3. The evolution of ice thickness and concentration for model runs with (a and c) and without (b and d) thermodynamics included. The horizontal axis is the distance along the transect shown in Fig. 2; the vertical axis is time.

$C_d^{ctrl} = 5 \times 10^{-3}$ is the value of the air–ice drag coefficient in the control run and $\mathscr{F}(A)$ is a monotonically varying function with $\mathscr{F}(A) \approx 2$ when $A < 0.4$ and $\mathscr{F}(A) \approx 1$ when $A > 0.6$. The function $\mathscr{F}(A) = 1/6\{9 + 2 \arctan[25(1 - 2A)]\}$ has this behaviour, and the steady state solution forced by along-channel wind stress is shown in Fig 5. An examination of the ice thickness and ice concentration fields shows that a clear transition region occurs in these fields at approximately 40 km along the channel. Viewing this transition region to be our polynya edge, we note that the velocity decrease across the edge is sharp and there is an equally sharp drop in the thermodynamic ice growth rate across the polynya edge.

However, it should be emphasized that the results in Fig 5 are obtained with an ad-hoc change in the air–ice drag coefficient. Although there are clear physical processes that can give rise to fast moving frazil ice and slower consolidated ice, we do not know of any quantitative theory for this. Ideally, one would like to have a theory for determining $\mathscr{F}(A)$. We expect the function $\mathscr{F}$ to produce an increase in ice–water drag for lower concentrations, with a rapid decrease in drag occurring at some critical concentration A_c (here $A_c = 50\%$). Finally, the decrease in the drag coefficient for this theory would have to be relatively sharp in the neighbourhood of A_c, otherwise a distinct polynya edge would be lost. The experiment shown in Fig. 5 is an exploratory one; this air–ice drag coefficient parameterization is not used in subsequent results presented below. In the following subsection where we examine cases with on-shore winds, the fixed control value of the air–ice drag coefficient is used.

In summary, a steady state ice cover is reached in the control run, with thinner ice towards the upwind shore. However, a clearly identifiable polynya edge is missing. This is not surprising,

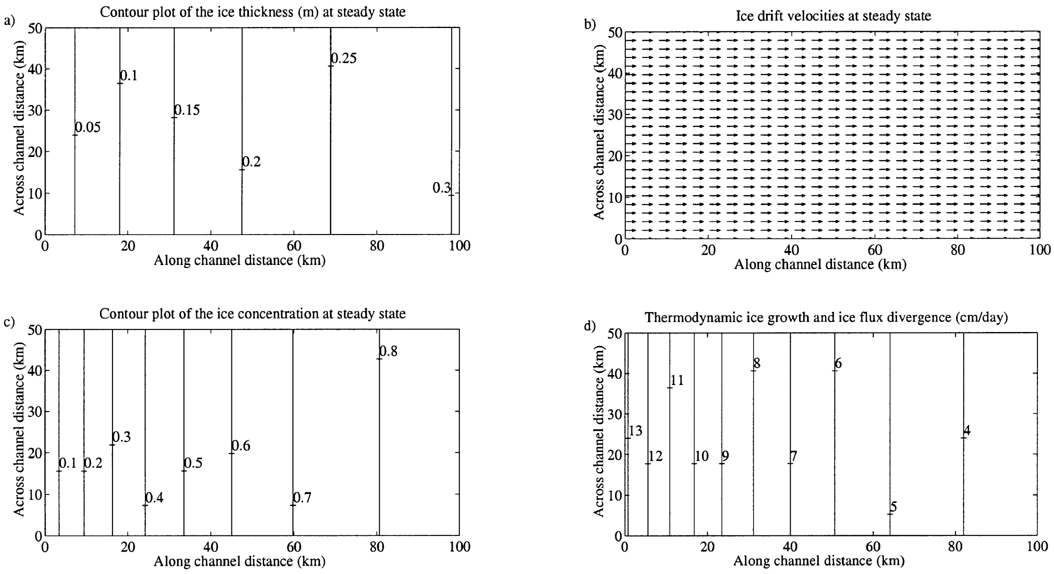

Fig. 4. Steady state fields obtained for the (a) ice thickness, (b) ice drift velocity, (c) ice concentration and (d) ice flux divergence. In (b) the uniform speed of the ice is 26 cm/s.

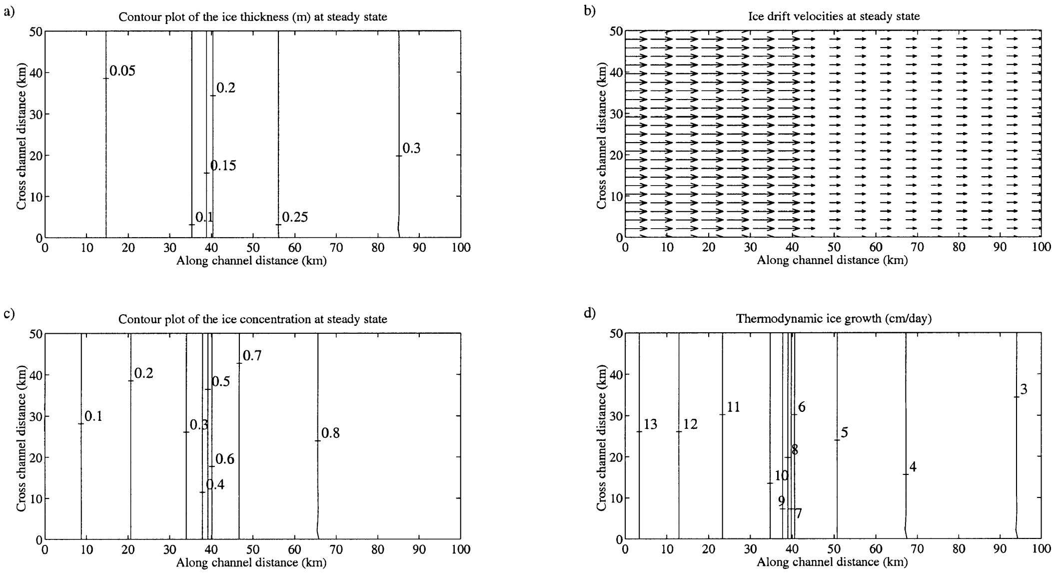

Fig. 5. Steady state fields obtained when the air drag on the ice depends monotonically on the ice concentration. Shown are: (a) ice thickness, (b) ice drift velocity, (c) ice concentration and (d) thermodynamic ice growth rate. In (b) the ice velocity is 52 cm/s in the left part of the domain, but 26 cm/s in the right part.

because the along-channel ice flow is completely unobstructed. If the air–ice drag is enhanced when the ice concentration is low, one can obtain a distinct polynya edge without introducing obstructions to the flow. Such parameterizations are premature, however, as a quantitative theory for the frazil ice velocity is lacking. However, for winds with an on-shore component, enhancement of the air–ice drag is not required to obtain a distinct polynya edge because the consolidated ice will be slowed down when internal ice stresses become significant in a region adjacent to the coast where ice convergence occurs.

3.2. *Solutions with varying wind direction*

The next suite of experiments consisted of runs where the wind direction was varied. Instead of setting $\theta = 0°$, as in the previous section, we consider the cases $\theta = 30°$, $45°$ and $60°$.

Fig. 6 shows the fields of ice thickness, ice velocity, ice concentration and thermodynamic growth rate (which, by (10), is equal to the ice flux divergence in the steady state) obtained after 50 model days of integration with $\theta = 30°$. In this case the ice no longer drifts along-channel everywhere, but instead drifts with an on-shore component with respect to the boundary $y = 50$ km (Fig. 6b). This ice flow opens up the polynya to the north and east of the boundaries $y = 0$ (south wall of channel) and $x = 0$ (end wall of channel) respectively, and results in an asymmetric polynya with ice build-up in the remainder of the domain. In the polynya region the thickness (Fig. 6a) is low (less than 0.2 m), the concentration (Fig. 6c) is less than 50%, the ice velocity (Fig. 6b) is in free drift (oriented along the wind direction) and the rate of thermodynamic ice growth (Fig. 6d) is high (more than 7 cm/day). In the consolidated ice region the ice is thicker (greater than 0.25 m), it is almost fully concentrated, the drift is down-channel and the ice production rate is quite low (less than 3 cm/day). The polynya edge appears in the above fields as a front that separates the two regions and is extremely well defined (has a sharp spatial gradient). It is also clear that the polynya edge does not asymptote to the southern domain wall, but rather it equilibrates at around 10 km off-shore from the boundary $y = 0$ (at about 60 km down the channel). This 10 km distance is the Lebedev–Pease width ($L_p = HV/\bar{F}$) for frazil ice emanating from the southern wall.

We obtained similar results when the wind stress is oriented at 45° and 60° from the channel axis. Fig. 7a–d shows the ice thickness and concentration obtained in these cases. In each case, the results showed two distinct regimes, the polynya and the consolidated ice, separated by a sharp polynya edge. The ice velocity and thermodynamic ice growth for these wind directions (not shown) were analogous to those obtained for 30° wind (i.e., both fields exhibited sharp changes across the polynya edge). For the velocity there was a sharp change in the direction of the ice flow across the polynya edge (from along-the-wind flow to along-the-channel flow), and the speed of the flow was

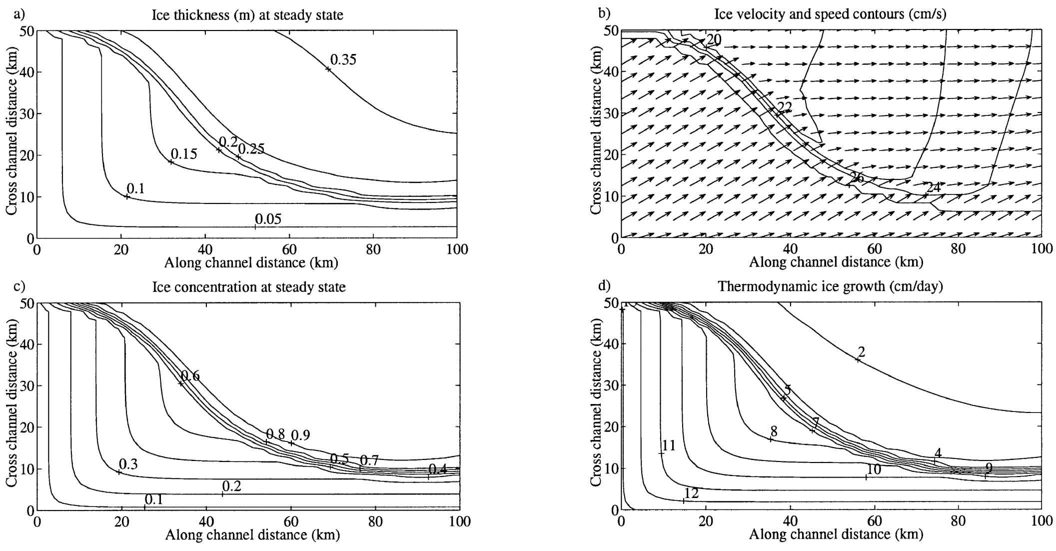

Fig. 6. Steady state obtained with $\theta = 30°$. Shown are: (a) ice thickness, (b) ice drift velocity, and contours of the drift speed, (c) ice concentration and (d) thermodynamic ice growth rate.

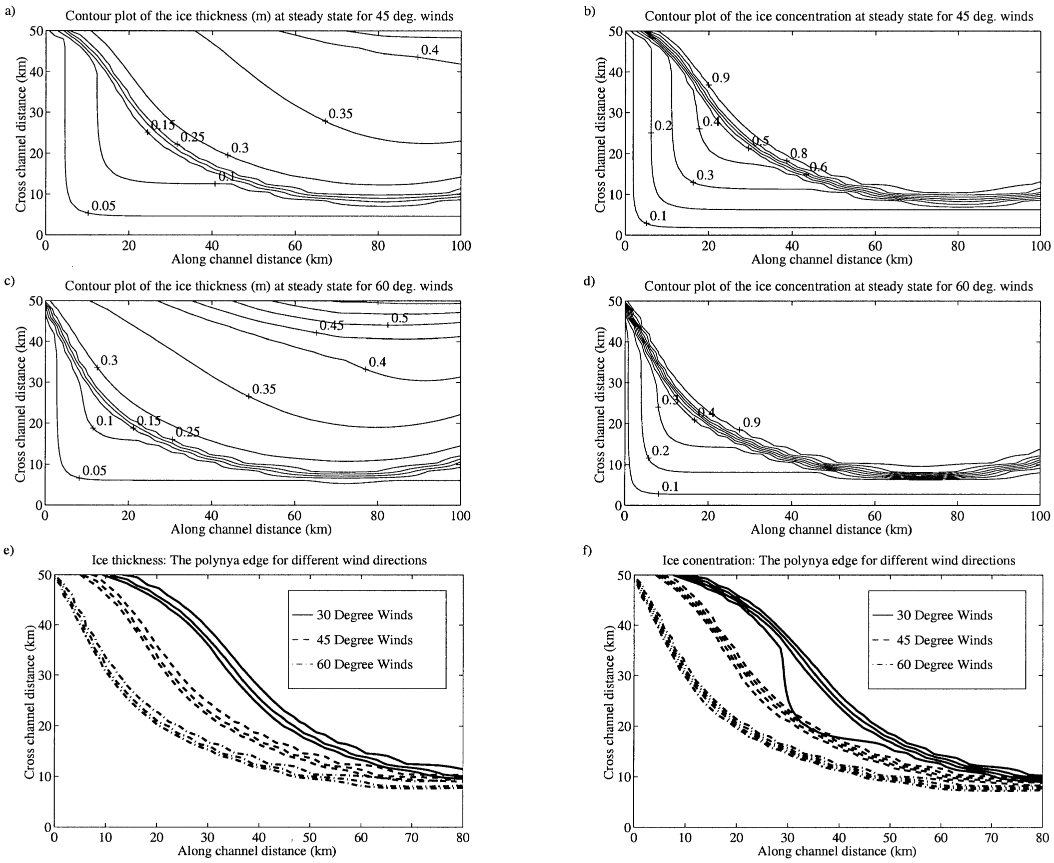

Fig. 7. Top and mid panels: Steady state results for 45° and 60° winds. Shown are ice thickness and concentration for 45° winds (a, b), and ice thickness and concentration for 60° winds (c, d). Bottom panels: A comparison of the polynya edge position for the different wind directions. Shown in (e) are the 0.2, 0.24 and 0.28 m ice thickness contours, and in (f) the 50%, 60%, 70% and 80% contours for ice concentration.

lower in the consolidated ice. Thermodynamic ice growth was high in the polynya, but at the edge it dropped sharply. From examining the ice thickness fields (Fig. 7a, c) and comparing these with the ice thickness obtained with 30° winds (Fig. 6a), we note that the thickness of the consolidated ice increases with θ. This is not surprising, because increasing θ leads to greater pressure against the north wall of the channel. For all solutions with non-zero θ the ice concentration is already more than 90% throughout the consolidated ice region, and hence it does not increase in the same manner as the ice thickness.

A close examination of Fig. 7c, d reveals that beyond 90 km along the channel the polynya edge curves away from the southern wall. This effect, which can also be seen in the results obtained with 45° winds, but is hardly noticeable in the results using 30° winds, is purely an edge-effect associated with the open boundary. Close to the open boundary internal stresses in the ice are reduced, leading to higher across-channel velocities at the edge, and hence a larger Lebedev–Pease width. This effect vanished in the model domain (from 0 to 100 km along channel) in sensitivity experiments in which we moved the open boundary to $x = 240$ km.

Fig. 7e, f shows the location of the polynya edge for all three non-zero values of θ. Due to the open boundary effect the polynya edge is only plotted to $x = 80$ km. We first note that the polynya edge moves closer to the end-wall of the channel (at

$x=0$) as the wind angle increases. Along the transect shown in Fig. 2 the polynya edge lies at around 15 km away from the end-wall for 60° winds, and it is close to 30 km and 45 km away from the wall for the cases of 45° and 30° winds, respectively. It is anticipated that the polynya edge would move closer to the end-wall as the along-channel component of the wind is reduced; however, it is surprising by how much it moves. If the position of the edge was proportional to the along-channel component of the wind we would expect the edge to lie at 15, 21 and 26 km offshore for the cases of 60°, 45° and 30° winds respectively. In all cases the polynya edge equilibrates close to 10 km from the southern domain wall. This shows that the Lebedev–Pease width for the frazil ice emanating from the southern wall is essentially the same for all wind directions. This is also interesting, since one might expect the across-channel consolidated ice velocity (V) at the polynya edge to increase with the across-channel component of the wind. The fact that this does not happen, shows that V is constrained. In the following subsection we study this feature in more detail, when we compare the ice model results to those obtained with a flux model.

3.3. *Comparison with the flux model*

We used the above results from the ice model to calculate the position of the polynya edge using the flux model of WMMD. We performed this calculation for both 30° and 45° winds.

To apply the flux model we need values for the frazil ice velocity (u, v), the consolidated ice velocity (U, V), the thickness of the consolidated ice H and the frazil ice production rate F (see Subsection 2.1 for details). In Fig. 6b there are two distinct velocity fields which will be viewed as corresponding to frazil ice (i.e., the velocity field inside the polynya) and the consolidated pack ice. By averaging spatially over these two areas we obtained mean values for the ice velocity components. Averaging the ice growth rate (Fig. 6d) inside the polynya region yields frazil ice production rate (F). Finally, the consolidated ice thickness at the polynya edge (H) is found by calculating the average consolidated ice thickness along the polynya edge. Table 2 shows the mean values that were obtained from these calculations both for the the 30° and the 45° winds.

Table 2. *Values used for the flux model, obtained as mean values from the 30° winds and the 45° experiments; the velocity components are in units of cm/s, H is in cm and F is in cm/day*

Variable	30° winds	45° winds
U	21.4	17.3
V	2.7	3.4
u	22.1	18.2
v	12.9	18.2
H	21.7	20.0
F	10.5	11.6

Fig. 8a shows the results obtained for the 30° winds. The dashed line in Fig. 8a shows the results obtained from the flux model with spatially varying consolidated ice velocity $[U(x, y), V(x, y)]$ and spatially varying frazil ice production rate $F(x, y)$. These fields are determined from the ice model, using bi-linear interpolation. In this case, due to mass conservation, the flux of ice at the polynya edge should be exactly the same for both models, as is apparent by the close agreement between the ice model (thin lines) and the flux model. Since F, U and V all exhibit spatial variability, we investigated as to whether these could be represented in the flux model by a spatial average. We found that close agreement was still obtained when when either $U(x, y)$ or $F(x, y)$ were replaced by their spatial averages. However, we also found that it was important to retain the across channel variation in V. The two other solutions in Fig. 8a show the flux model solution obtained for two different choices of the across-channel velocity component V with F and U fixed at their spatial averages. First, we averaged V in the along-channel direction across the consolidated ice, which produces a nearly linear profile $V(y)$ such that $V(L)=0$ and $V=5.5$ cm/s at the polynya edge. When we used the resulting $V=V(y)$ profile in the flux model we obtained the polynya edge shown by the dot-dashed curve. Although this solution is, overall, similar to the ice model edge it differs considerably from the former in the region between 30 km to 60 km downstream from the end wall of the channel. This curve does indeed approach the model polynya edge for $x \geqslant 60$ km, because in that region both models satisfy $(HV)/\bar{F} \approx 10$ km, the Lebedev–Pease width associated with the boundary $y=0$. The 3rd flux model solution shown in Fig. 8a was obtained with simply $V = 0$. In this case the flux model solution asymptotes towards the x-axis, which is to be expected, as the Lebedev–Pease width vanishes when $V = 0$.

Fig. 8b shows the comparison for the case of 45° winds. The conclusions are the same as for the 30° winds (i.e., with full spatial variability in all model fields, we obtain very close agreement between the ice model and the flux model). Experiments with different across-channel velocities (V) again revealed that it was sufficient to specify only the across-channel variation (i.e., $V = V(y)$) to get a fairly good comparison.

To summarize, the results in this subsection show that there is good agreement between the ice model and the flux model when the input fields for the flux model are spatially varying. However, there is also reasonably good agreement when simply the across-channel variability in V is retained. The across-channel variability in V is dependent on the way that the build-up of internal stresses in the ice affect its motion, i.e., it depends on the model rheology. The above results, therefore show the importance of the ice model rheology in setting up the location of the polynya edge in the channel. In the following section we will perform various sensitivity experiments with the goal of gaining an understanding of how $V(y)$ (and thus the Lebedev–Pease width) depend on the model rheology.

4. Sensitivity to different formulation of ice dynamics

The results from the previous experiments show that the ice rheology becomes important in determining the shape of the polynya edge. This immediately leads to the question whether a different polynya size and shape would be obtained with different rheologies. Furthermore, for a given rheology, how sensitive is the polynya to the parameters of the rheology? In this section we present the results from several sensitivity experiments that were performed, with the goal of elucidating the role of ice rheology in determining the shape and size of the polynya. All experiments in this section use 30° winds.

4.1. Sensitivity to rheology parameters

One crucial aspect of the ice model rheology is that internal pressure in the ice is limited to a maximum compressive load P^c_{max}. If the internal ice pressure exceeds P^c_{max}, the ice will form ridges. Following Hibler (1979) the ice model of TM parameterizes the dependence of P^c_{max} on ice thickness (h) and concentration (A) by

$$P^c_{max} = P^* h \exp[-C(1 - A)],$$

where P^* and C are free parameters. In previous experiments $P^* = 5000$ Pa and $C = 30$ are used as the control values. To examine the sensitivity of the ice model polynya to changes in P^c_{max}, we performed three experiments. In the first one C was halved, but P^* kept as before (at 5000 Pa); in the next two experiments C was kept as before (at 30), but P^* was first doubled, and then halved. The results are shown in Fig 9.

An examination of Fig. 9 shows that the results are not sensitive to a reduction in C or an increase in P^*. However, the results show some sensitivity to a reduction in P^*. With P^* halved the ice becomes thicker up against the northern coast. This is simply the result of ridging, as with a lower

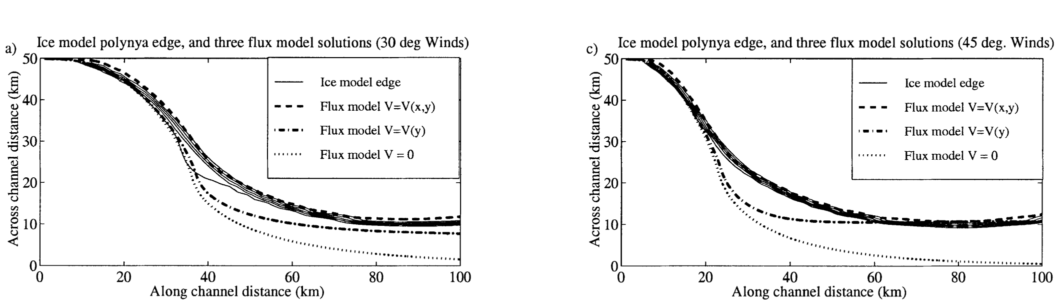

Fig. 8. Comparison of the flux model and the sea ice model. Plot (a) shows ice model results (for ice thickness) for 30° winds and three flux model (FM) solutions. Plot (b) is the same as (a) but for 45° winds.

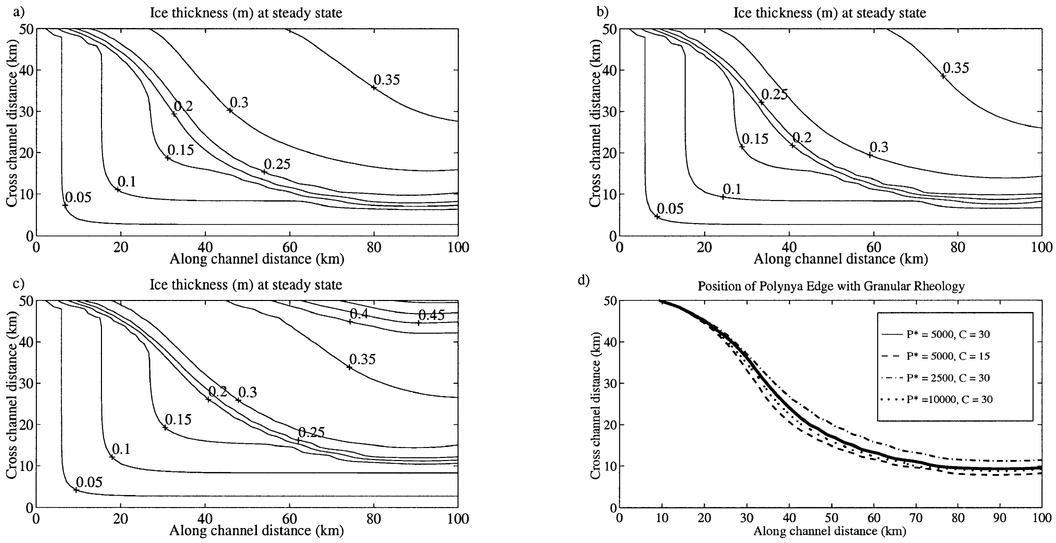

Fig. 9. Steady state ice thickness results obtained with $\theta = 30^\circ$ and for three different combinations of $P^c_{\max}$ parameters. Shown are: (a) the results for the case with $C = 15$ and $P^* = 5000$ Pa; (b) the results obtained with $C = 30$ and $P^* = 10{,}000$ Pa; and (c) the results obtained with $C = 30$ and $P^* = 2500$ Pa. Plot (d) shows the position of the polynya edge in each case and in the control case ($P^* = 5000$ and $C = 30$).

P^*, the ice can tolerate less compressive load before it starts to ridge. This increase in h partially offsets the reduction in P^*. We note that the thickness increase is in an area where the ice has a high concentration, which explains why a similar ridging did not occur when C was halved. In (9) when $A \approx 1$ we will have, $P^c_{\max} \approx P^* h$ regardless of what value we have for C. In the control run there was little ridging that took place in this part of the domain, which explains why doubling P^* has such a small effect.

4.2. *Sensitivity to rheological formulation*

In the TM model, the maximum shear stress supported by the sea ice is $P^s_{\max} = P^c_{\max} \times \sin\phi$, where $\phi = 30^\circ$ is the internal friction angle. If the friction angle is set to zero the ice will loose all shear strength ($P^s_{\max} = 0$). Such a case is known as cavitating sea ice rheology and has been implemented in ice models (Flato and Hibler, 1992). The results obtained with this rheology are shown in Fig. 10a, and are quite similar to those obtained with granular rheology (Fig. 6a).

There are subtle differences in the position of the polynya edge which are evident in Fig. 10b. Beyond 50 km in the along-channel direction, the Lebedev–Pease width obtained with a cavitating ice model is larger than that obtained with granular rheology. The enhanced Lebedev–Pease width means that V at the polynya edge must be larger for the cavitating model. Thus the cavitating model, which has no shear strength, can support a larger across-channel gradient in V, than the granular fluid can.

4.3. *Sensitivity to boundary conditions*

The experiments thus far have used free-slip boundary conditions, which imply that there is no shear stress between the coast and ice that slides along it. Thus the flow along the coast is not impeded by the shear strength of the ice. Since we observed subtle differences between the results obtained with shear strength (granular rheology) and without shear strength (cavitating fluid), the question arises whether the ice velocity field and the position of the polynya edge using the granular rheology is sensitive to the free-slip boundary condition. Fig. 11 shows the results obtained when the control case with 30° winds (Fig. 6) was repeated using no-slip boundary conditions.

It is clear that using no-slip boundary conditions greatly reduces the ice drift velocities along

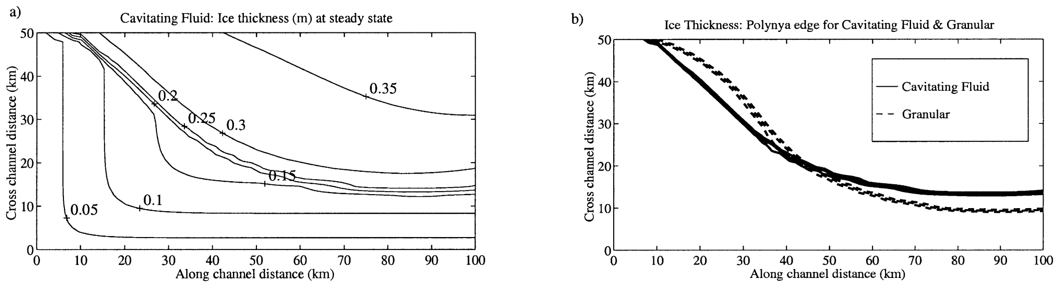

Fig. 10. (a) Steady state ice thickness obtained with cavitating fluid rheology and wind angle $\theta = 30^{\circ}$. (b) A comparison of the polynya edge position using granular rheology and cavitating fluid rheology. In (b) the 0.18, 0.20 and 0.22 m contours are plotted.

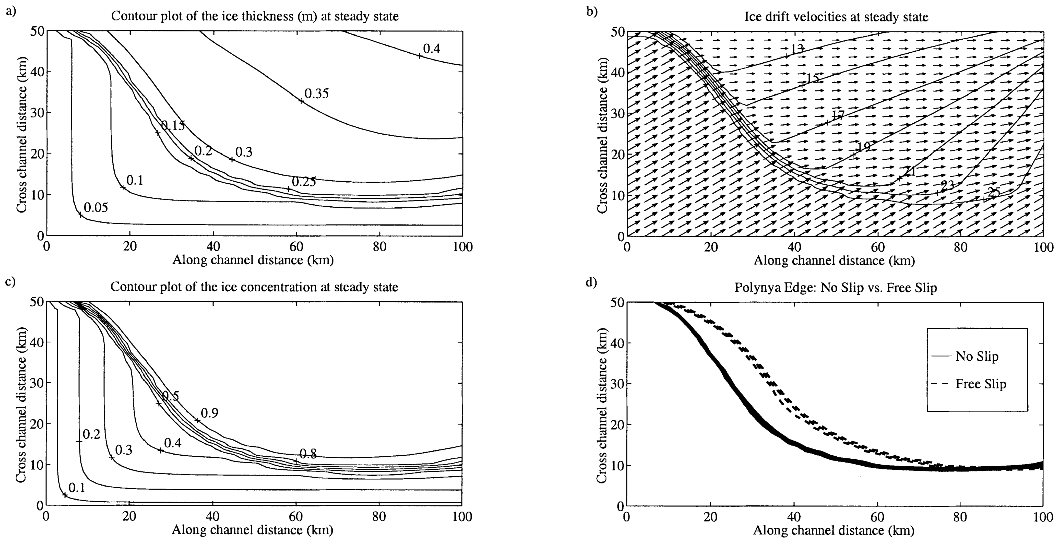

Fig. 11. Steady state solution obtained with no-slip boundary conditions. Shown are: (a) ice thickness, (b) ice drift velocity and contours of the drift speed, and (c) ice concentration. Plot (d) shows comparison of the polynya edge position for the no-slip and free slip cases. In (d), the 0.18, 0.20 and 0.22 m contours are drawn.

$y = L$. The mean consolidated ice speed is now 18 cm/s as opposed to 21 cm/s with free-slip boundary conditions. The reduction in the along-channel velocities near $y = L$ produces a smaller polynya, but other aspects of the polynya structure remain the same.

In summary, the results of this section shows that the ice model is not overly sensitive to the details of the model rheology. There is some sensitivity to the reduction of the ice strength parameter (P^*), and the lack of shear strength (as in a cavitating fluid) such changes will increase the Lebedev–Pease width for the southern boundary. Similarly, the polynya structure is overall not sensitive to whether free-slip or no-slip boundary conditons are used. In the next section we will show how these observations can be combined in a simple theoretical framework.

5. A simple theory for the polynya and the consolidated ice pack

The results of Section 3 showed that the ice model could produce a polynya with a sharp polynya edge provided there was convergence in the ice velocity field. When we ran the ice model with winds that had an onshore component, such a convergence region occurred in a transition zone between the polynya, where the ice is in free drift, and the consolidated ice region, where the ice flow is strongly influenced by internal stresses. However, the comparison with the flux model revealed that in the stress dominated region, it is only the across-channel change in V, the quantity most affected by internal stresses, which must be properly accounted for.

The sensitivity experiments of Section 4 showed that in general the polynya shape and size were not sensitive to the details of the model rheology. Motivated by these results we now develop a simplified theoretical framework to describe the flow of the consolidated ice. We will then combine this with the flux theory, and compare the outcome of the combined theory with the results of the ice model.

5.1. *A simplified solution for the consolidated ice flow*

To gain further understanding of the consolidated ice motion, we now examine how the internal pressure is distributed within the ice pack. In Subsection 3.3, we noticed that $V(y)$ decreased to zero almost linearly from the polynya edge to the wall at $y=L$. This decrease in V could lead to velocity convergence throughout the consolidated ice, and ridging would result. Alternatively, the divergence could be zero in the consolidated ice, in which case the the decrease in V would result in a down-channel increase in U (as indeed is observed in Fig. 6b). In the first case, the internal compressive load must be at P^{c}_{max}; in the second case, the internal pressure could be lower.

Fig. 12a shows the divergence of the ice velocity ($\nabla \cdot \boldsymbol{u}_i$) for the ice velocity ($\boldsymbol{u}_i$) shown in Fig. 6b. The polynya edge stands out in the figure, as a zone of convergence, but away from the polynya edge there is hardly any convergence or divergence. This is clear from Fig. 12b, which shows the value of the divergence along a transect at $x=50$ km. Since the ice velocities in the polynya are in free drift, we know that in the polynya the internal ice pressure must zero. At the edge where convergence occurs, clearly the internal compressive load must be at P^{c}_{max} $(=P^{*}h_{edge})$. In the consolidated ice the compressive load cannot be lower than that at the polynya edge. Comparison of Figs. 12a, b and Fig. 6a reveals that the divergence goes to zero close to the location of the 0.3 m contour of the ice thickness. The ice thickness at the coast is about 0.35 m and thus the internal compressive load throughout the bulk of the consolidated ice is between $P^{*}\times 0.3$ and $P^{*}\times 0.35$, and due to the stress exerted by the winds is likely to be closer to the latter value.

Fig. 12c shows the invariant shear strain rate given by

$$\frac{1}{2}\times\left[\left(\frac{\partial u}{\partial x}-\frac{\partial v}{\partial y}\right)^{2}+\left(\frac{\partial v}{\partial x}+\frac{\partial u}{\partial y}\right)^{2}\right]^{1/2}$$

for the ice velocity field of Fig. 6b. As with the divergence field, the polynya edge stands out as the region of greatest shear strain. Furthermore, there is no shear strain in the polynya, but in the consolidated ice small amounts of shear strain are observed (Fig. 12d). The fact that the shear strain rate is non-zero in the consolidated ice implies that the maximum shear stress (P^{s}_{max}) has been reached; the fact that it is small agrees with $V(y)$ being nearly linear.

The steady-state ice momentum balance for the consolidated ice block is

$$\boldsymbol{\tau}_a=\boldsymbol{\tau}_w-\nabla\cdot\boldsymbol{\sigma}, \tag{17}$$

upon neglecting the Coriolis and sea surface tilt terms. The form of the ice–water stress adopted in the numerical ice model is given by

$$\boldsymbol{\tau}_w=K_w\boldsymbol{u}_i, \tag{18}$$

where K_w is a constant. Suppose that the block occupies the region $0<l<y<L$, and define $d=L-l$. We assume that the along-channel velocity of the block can be represented by a mean value $\bar{U}$ and that the across-channel velocity, $V(y)$, varies linearly from a maximum value (V_m) at the polynya edge to zero at the coast. Furthermore, in the stress tensor we neglect variations in the along-channel direction thus $\boldsymbol{\sigma}=\boldsymbol{\sigma}(y)$. In component form, (17) becomes:

$$\tau^{x}=K_w\bar{U}-\frac{\partial\sigma_{xy}}{\partial y}, \tag{19}$$

$$\tau^{y}=K_wV(y)-\frac{\partial\sigma_{yy}}{\partial y}, \tag{20}$$

where the uniform wind stress $\boldsymbol{\tau}_a=(\tau^{x},\tau^{y})$.

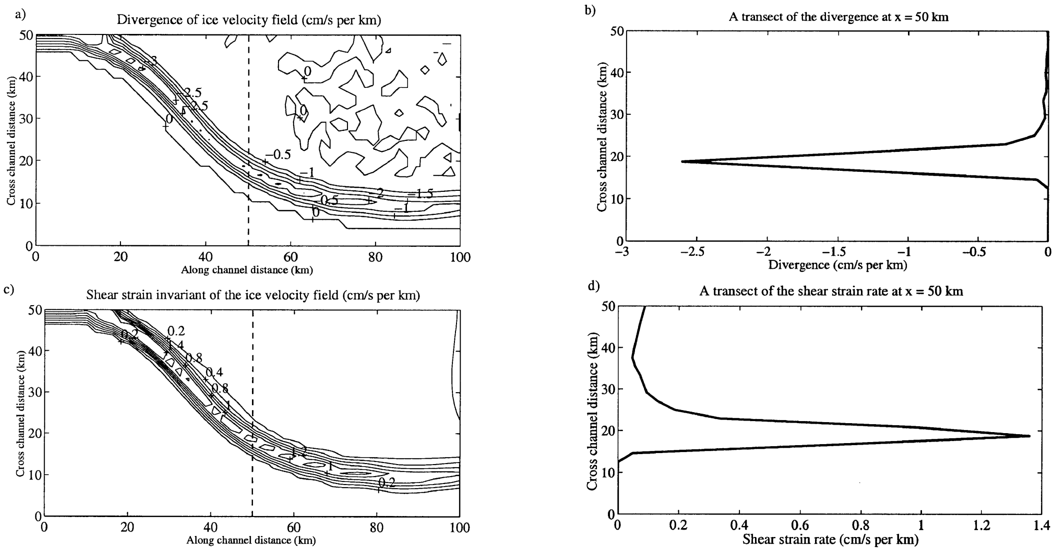

Fig. 12. The divergence of the ice velocity field (a) and the invariant shear strain rate of the ice velocity field (c). A transect through (a) at $x = 50$ km is shown in (b) and a similar transect through (c) is shown in (d). The thin dashed vertical line in (a) and (c) is the location of transects shown in (b) and (d).

Integrating (19) from $y = l$ to $y = L$ yields

$$(K_\mathrm{w}\bar{U} - \tau^x)d = \sigma_{xy}(L) - \sigma_{xy}(l). \tag{21}$$

In accordance with what we know about the internal pressure state, we assume that the boundary $y = l$ is stress-free (this is true if we extend the integration a short distance into the polynya) and that $\sigma_{xy}(L) = -P^\mathrm{s}_\mathrm{max}$, the maximum shear-stress. With these assumptions (21) gives

$$\bar{U} = \frac{1}{K_\mathrm{w}}\left(\tau^x - \frac{P^\mathrm{s}_\mathrm{max}}{d}\right). \tag{22}$$

Strictly speaking (22) is only valid for no-slip boundary conditions for free-slip boundary conditions, we have $\sigma_{xy} = 0$ which reduces (22) to free drift in the down-stream direction.

Similarly, integrating (20) with respect to y yields

$$\left(K_\mathrm{w}\frac{V_\mathrm{m}}{2} - \tau^y\right)d = [\sigma_{yy}(L) - \sigma_{yy}(l)], \tag{23}$$

where we have used the assumption that $V(y)$ varies linearly from zero to a maximum value (V_m) across the block. From the previous analyses we know that at the coast the pressure is close to the maximum compressive load $\sigma_{yy}(L) = -P^\mathrm{c}_\mathrm{max}$, and that $y = l$ is a stress-free boundary. This allows (23) to be written as

$$d = \frac{P^\mathrm{c}_\mathrm{max}}{\tau^y - K_\mathrm{w}V_\mathrm{m}/2}. \tag{24}$$

If the thickness of the ridging ice adjacent to the coast is H_r, then $P^\mathrm{c}_\mathrm{max} = H_\mathrm{r}P^*$ and $P^\mathrm{s}_\mathrm{max} = P^\mathrm{c}_\mathrm{max}\sin\phi$. The windstress $\boldsymbol{\tau}_\mathrm{a} = (\tau^x, \tau^y)$ is prescribed, and if V_m is also known, we can calculate d from (24) and $\bar{U}$ from (22). However, V_m can also be related to d through the Lebedev–Pease width

$$L - d = l = \frac{V_\mathrm{m}H}{F}, \tag{25}$$

where H is thickness of the consolidated ice at the polynya edge. Using (25) to eliminate V_m in (24), we can obtain a quadratic equation for d:

$$d^2 + \left(\frac{2H\tau^y}{K_\mathrm{w}F} - L\right)d - \frac{2HP^\mathrm{c}_\mathrm{max}}{K_\mathrm{w}F} = 0. \tag{26}$$

Inspection of (26) shows that this has real solutions, one of which is positive. Using (26) to find d, V_m can then be found either from (24) or (25), and finally $\bar{U}$ can be found from (22).

As a test of this theory, we use the parameters from Table 1, a linear drag law and 30° winds to obtain the following· $\boldsymbol{\tau}_a = K_a|\boldsymbol{v}_a|(\sqrt{3}, 1)/2$, where $K_a = \rho_{air} C_{da} = 6.5 \times 10^{-3}$ is the net atmospheric drag, and $|\boldsymbol{v}| = 20$ m/s is the wind speed. The ice–ocean drag is $K_w = \rho_w C_{dw} = 0.5$ and the maximum compressive load is

$$P^c_{max} = P^* H_r = 5000 \text{ N m}^{-2} \times 0.35 \text{ m} = 1750 \text{ N/m}.$$

The thickness of the consolidated ice at the polynya edge is $H = 21.0$ cm and the frazil ice production rate is $F = 10.5$ cm/day. Then (26) yields $d \approx 37.5$ km, which is close to the 40 km width of the consolidated ice, shown in Fig. 6. When calculating $\bar{U}$ from (22), we can either use free-slip boundary conditions (and simply neglect the P^s_{max}/d term in (22)) or use no-slip boundary conditions and

$$P^s_{max} = P^c_{max} \sin\phi = 875 \text{ N/m}.$$

The free-slip calculation gives $\bar{U} \approx 22$ cm/s and the no-slip calculation gives $\bar{U} \approx 18$ cm/s. Both of these values agree quite well with the values previously obtained from the model results (see Subsections 3.3 and 4.3, respectively). Finally, we calculate V_m from (25) and obtain 7 cm/s, a value somewhat higher than the 5.5 cm/s obtained from the model results in Subsection 3.3.

Two assumptions in the above analysis are critical. First, we assumed that the stresses do not vary in the along-channel direction. Clearly this assumption is not strictly valid, especially in the region where the thickness of the consolidated ice is changing. Furthermore we assumed that U could be represented by a mean value, even though we know (from the zero divergence of the consolidated ice velocity) that U must increase down the channel. A fully consistent approach would be to integrate (17) over the entire consolidated ice region. Using the divergence theorem and demanding that stresses vanish on the polynya edge and at the open end of the channel, one obtains:

$$\tau^x = K_w \bar{U} - \frac{1}{A_c} \int_{\gamma_1}^{\gamma_2} \sigma_{xy}(x, L)\, dx, \tag{27}$$

$$\tau^y = K_w \bar{V} - \frac{1}{A_c} \int_{\gamma_1}^{\gamma_2} \sigma_{yy}(x, L)\, dx, \tag{28}$$

where A_c is the area of the consolidated ice, $\bar{U}$ and $\bar{V}$ are the areal averages of U and V and the γ's mark the limits of consolidated ice in the along-channel direction. From these equations we can estimate how significant along-channel variations in $\boldsymbol{\sigma}$ are. Since $\sigma_{yy}(x, L)$ and $\sigma_{xy}(x, L)$ are assumed to be at the internal maxima (P^c_{max} and P^s_{max} respectively) $\sigma_{yy}(x, L)$ and $\sigma_{xy}(x, L)$ will vary in the same manner as the ice thickness along the northern coast $[h(x, L)]$, a quantity that exhibits small variations for free-slip conditions (Fig. 6a), but larger variations for no-slip boundary conditions (Fig. 11a).

To test how sensitive the value for $\bar{U}$ was to stress variations in the along-channel direction we used (27) to calculate $\bar{U}$ for the no-slip boundary conditions (Fig. 11). To estimate A_c we calculated the area where ice concentration exceeds 60% and obtained $A_c \approx 2900$ km^2. Using the same values as above for $\boldsymbol{\tau}_a$ and K_w and integrating

$$\sigma_{xy}(x, L) \approx P^s_{max}(x, L) = P^c_{max}(x, L) \sin\phi,$$

along the northern wall ($y = L$) we obtained $\bar{U} \approx 17$ cm/s, a value close to the 18 cm/s obtained previously. The limits of the integral where chosen as $\gamma_1 = 10$ km and $\gamma_2 = 100$ km. To choose the value for γ_1 we first examined the gradient of the ice thickness field adjacent to the northern wall (the x-component of the gradient, i.e, $\partial h(x, L)/\partial x$). This quantity showed a sharp peak between $x =$ 5 km and $x = 10$ km — the location of the polynya edge at the northern wall. Therefore, it is reasonable to pick $x = 10$ as the leading edge of the consolidated ice pack along the northern wall. Using (28) and

$$\sigma_{yy}(x, L) \approx P^c_{max}(x, L) = P^* h(x, L)$$

to calculate $\bar{V}$ yielded $\bar{V} \approx 1.6$ cm/s. This estimate of $\bar{V}$ does not depend on any assumptions about the across channel velocity structure, however it is not very useful for obtaining a value of V_m, unless assumptions about the structure of $V(y)$ be introduced again.

We are now in a position to understand why varying the wind angle had such a large effect on the position of the polynya near the end wall of the channel (see 3.2). As the wind angle increased the pressure on the northern coast (between 15 to 50 km in the along-shore direction) increased, and thus the thickness of consolidated ice block increased. This resulted in the polynya edge moving closer to the end wall of the channel (Figs. 6, 7) as the wind angle increased, by an amount that exceeded what what one would have expected from simply the changes in the along-channel component of the wind. Finally, when we used the cavitating fluid rheology, a smaller value for d is obtained than with granular rheology. Since the cavitating fluid does not support shear stress, we expect the pressure on $y = L$ to be reduced, and hence the value of d to be reduced, which is what is observed in Fig 10.

5.2. *Application to a flux model and comparison with ice model*

The analysis of the preceding section predicts the mean along-channel speed and across-channel width of the consolidated ice block, provided we are given H. Thus, the consolidated along-channel ice flux is determined and we can calculate the polynya edge using the WMMD model. In addition, we can also plot the analytical polynya edge solution associated with the special case $\boldsymbol{U} = (\bar{U}, 0)$. In both cases the polynya edge consists of two curves, which are shown in Fig 13. The first, C_1 is associated with frazil ice trajectories emanating from the end wall ($x = 0$) of the channel (see the left part of Fig. 13. Clearly C_1 passes through $(0, L)$ and terminates at the point $P = (x_p, y_p)$, where C_1 intersects the frazil ice trajectory which passes through the origin. Curve C_2 which smoothly joins C_1 at P, is associated with frazil ice trajectories emanating from the channel wall $y = 0$. We first consider the analytical solution for C_1 and C_2 when $\boldsymbol{U} = (\bar{U}. 0)$.

On C_1, $h_C = Fx/u$, which upon substituting into (3) and integrating yields

$$y - L = x \tan\theta + L_p \tan\theta \ln(1 - x/L_p), \tag{29}$$

where $\tan\theta = v/u$ is the orientation of the frazil ice trajectories and $L_p = H\bar{U}/F$ is the Lebedev–Pease width.

The point P is where the frazil ice trajectory $y = x\tan\theta$ intersects (29) and has coordinates given by

$$x_p = L_p[1 - \exp(-\mu\cot\theta)], \qquad y_p = x_p \tan\theta,$$

where $\mu = L/L_p$.

Now consider C_2 which passes through P. On C_2, $h_C = Fy/v$, which upon substitution into (3) and integrating yields:

$$y - y_p = (x - x_p)\tan\theta + L_p \tan\theta \ln(y/y_p). \tag{30}$$

When $\boldsymbol{U} = [\bar{U}, V(y)]$ and $V(y)$ is a linear function, an analytical solution can again be obtained. However, it does not yield further insight than that already given by (29) and (30). Fig. 13 shows a comparison of the above theory and the sea ice model results for the case of 30° winds. The results shows that the parameters obtained with the method outlined in the previous section give good

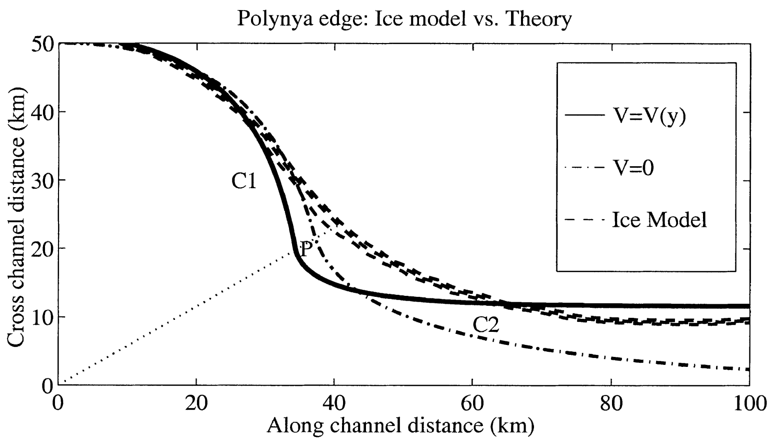

Fig. 13. Comparison of an ice model polynya edge and flux model polynya edge solutions. Plotted are: the polynya edge from the ice model (dashed contours of 18, 20 and 22 cm thicknesses), the polynya edge obtained with the WMMD flux model using $V_m = 7$ cm/s (solid) and the analytical flux model solution (dot–dashed). Also shown is the frazil ice trajectory emanating from the origin, the two parts of the polynya edge (C_1 and C_2) and also the point P, where C_1, C_2 and the frazil ice trajectory emanating from the origin intersect.

results for the polynya edge. For the WMMD model the polynya edge asymptotes to the Lebedev–Pease width (≈ 13 km) associated with frazil ice trajectories emanating from the channel wall $y = 0$. The polynya edge in the analytical model (where $V = 0$) asymptotes to the channel wall $y = 0$. The point P lies very close to the predicted Lebedev–Pease width (≈ 38 km) for frazil ice emanating from the end wall ($x = 0$) of the channel.

6. Conclusions and discussion

This paper had three goals. First, we wanted to understand polynya formation in a thermodynamic-dynamic sea ice model. Secondly, we wanted to determine to what extent a polynya in a sea ice model could be reproduced in a simpler flux model and what parameters were needed to reproduce the results of the ice model. Finally we wanted to combine the results of the two first two approaches and use a simple theory for the consolidated ice to calculate the parameters needed for the flux model.

As the ice model does not have implicit ice types, consolidated and frazil ice must emerge in the model results as different ice flow regimes, resulting from processes within the model. Furthermore, to obtain a polynya edge the boundary between the two regimes must be clearly defined. We have shown that to generate a well defined polynya edge, the ice model results must contain a zone of strong convergence, with an abrupt drop in ice speed and concomitant increase in ice thickness and concentration. Given this, a realistic drop in the ice production rate will occur across the polynya edge. We have shown that for ice that is unencumbered by internal stresses this convergence can be achieved by prescribing a concentration-dependent air–ice drag, and in cases where the wind has an on-shore component this convergence arises simply due to the build-up of internal stresses in the ice that is pushed against the coast. Comparing the ice model results with a polynya flux model indicated that the only dynamical variable whose details were important for the shape and size of the polynya was the across-channel velocity (V), which is the quantity most constrained by the domain shape, and thus is greatly affected by the model rheology. The polynya size and shape are relatively insensitive to the spatial variations of other fields.

By making simplifying assumptions about the distribution of stresses in the consolidated pack, we developed a simple description of how the pressure distribution in the consolidated ice pack affects the size of the ice pack and thus the size of the polynya. Using this to calculate parameters for the flux model, we were able to obtain a polynya edge that agreed quite well with the ice model.

Several outstanding issues remain. First, the results highlight the requirement for a parameterization of frazil ice transport through changes in the air–ice drag and possibly the ice–water drag. Secondly, the theory developed for the influence of rheology on the motion of the consolidated ice region, and hence the polynya, makes several simplifying assumptions, and further work is required to see if the theory can be extended to predict the ice pressure within the pack and an analytic form for the across-channel velocity profile, given the wind stress. Furthermore, it has been noted in several places that determining the pile-up thickness, H, of consolidated new ice at the polynya edge is problematic. Biggs et al. (2000) recognize this problem and have developed a parameterization for H in terms of frazil ice thickness (for the frazil ice arriving at the polynya edge) and ice dynamics. In Biggs et al. (2000) the collection depth now becomes one of the unknowns to be calculated in the flux model. The parameterization does not contain any unknown parameters, and it would be worthwhile to adopt it in an extension to this study.

This study was initiated as part of the international North Water Polynya Project (1997–2001). Even though the simplified domain used here is different from the NOW region, the salient features of this study are relevant to the formation of this polynya. Wind stress in the NOW is frequently directed towards Ellesmere Island, driving ice both equatorward and on-shore. We would therefore expect the sea ice rheology to be important in the region of coastal ice convergence, and the ice motion in this study captures the behaviour of that in the NOW. The polynyas calculated in this study are qualitatively similar in shape to the NOW.

It would be worthwhile to use ice concentration and velocity data in Baffin Bay in combination with a dynamic/thermodynamic sea ice model to investigate whether internal ice stresses are indeed responsible for creating the ice velocity convergence at the edge of the NOW. Although modelling studies (Darby et al., 1994) suggest that sensible heat associated with upwelling along the west Greenland coast plays a minor role in maintaining the NOW, there is still some lingering doubts about this conclusion. To resolve the issue we suggest that a state-of-the-art NOW model should be developed, comprising of a dynamic–thermodynamic sea ice model (e.g., the TM model) coupled to a wind and buoyancy driven OGCM. Hydrographic and current meter data collected by the International NOW Project should be used to validate the model.

7. Acknowledgements

This work was partly supported by a grant from the "NOW (North Water) Research Network," funded by NSERC. H. Bjornsson was also partly supported by an NSERC Research Grant awarded to L. A. Mysak. H. Bjornsson acknowledges the support of the AOS visiting scientist program at Princeton University. A. J. Willmott acknowledges the award of a Keele University Research Award while carrying out this research. AJW and M. A. Morales Maqueda gratefully acknowledge support from the UK NERC via a research grant awarded by the fourth round of the Antarctic Special Topic Awards. We are grateful to the anonymous reviewers whose comments led to improvements of this paper and also to Bruno Tremblay for supplying us with the updates to his sea ice model and for useful discussions.

REFERENCES

Aagard, K. L., Coachman, K. and Carmack, E. 1981. On the halocline of the Arctic Ocean. *Deep-Sea Res.* **28**, 529–545.

Biggs, N. R. T., Morales Maqueda, M. A. and Willmott, A. J. 2000. Polynya flux model solutions incorporating a parameterization for the collection thickness of consolidated new ice. *J. Fluid Mech.* **408**, 179–204.

Brandon, M. A. and Wadhams, P. 1999a. The near surface hydrography beneath the Odden ice tongue. *Deep-Sea Res.* **II 46**, 1427–1455.

Brandon, M. A. and Wadhams, P. 1999b. The physical properties of sea ice in the Odden ice tongue. *Deep-Sea Res.* **II 46**, 1475–1500.

Cavalieri D. J. and Martin, S. 1994. The contribution of Alaskan, Siberian and Canadian coastal polynyas to the cold halocline layer of the Arctic Ocean. *J. Geophys. Res.* **99**, 18,343–18,362.

Chapman, D. C. 1999. Dense water formation beneath a time-dependent coastal polynya. *J. Phys. Oceanogr.* **29**, 807–827.

Chapman, D. C. and Gawarkiewicz, G. 1997. Shallow convection and buoyancy equilibrium in an idealized coastal polynya. *J. Phys. Oceanogr.* **27**, 555–566.

Darby, M. S., Willmott, A. J. and Mysak, L. A. 1994. A nonlinear steady state model of the north water polynya, Baffin Bay. *J. Phys. Oceanogr.* **24**, 1011–1020.

Darby, M. S., Willmott, A. J. and Sommerville, T. 1995. On the influence of coastline orientation on the steady state width of a latent heat polynya. *J. Geophys. Res.* **100**, 13,625–13,633.

Fichefet, T. and Goosse, H. 1999. A numerical investigation of the spring Ross Sea polynya. *Geophysical Research Letters* **26**, 1015–1018.

Flato, G. M. and Hibler, III, W. D. 1992. Modeling pack ice as a cavitating fluid. *J. Phys. Oceanogr.* **22**, 626–651.

Grumbine, R. W. 1991. A model of the formation of high-salinity shelf water on polar continental shelves. *J. Geophys. Res.* **96**, 22,049–22,062.

Hibler, III, W. D. 1979. A dynamic thermodynamic sea ice model. *J. Phys. Oceanogr.* **9**, 815–846.

Kampf, J. and Backhaus, J. O. 1999. Ice–ocean interaction during shallow convection under conditions of steady winds: three dimensional numerical studies. *Deep-Sea Res.* **II 46**, 1335–1355.

Lebedev, V. L. 1968. Maximum size of a wind generated lead during sea freezing. *Oceanol.* **8**, 313–318.

Lynch, A. H., Glueck, M. F., Chapman, W. L., Bailey, D. A. and Walsh, J. E. 1997. Satellite observation and climate system model simulation of the St. Lawrence Island polynya. *Tellus* **49**, 277–297.

Morales Maqueda, M. A. and Willmott, A. J. 2000. A two-dimensional time-dependent model of a wind-driven coastal polynya: application to the St. Lawrence Island polynya. *J. Phys. Oceanogr.* **30**, 1281–1304.

Ou, H. W. 1988. A time-dependent model of a coastal polynya. *J. Phys. Oceanogr.* **18**, 584–590.

Pease, C. H. 1987. The size of wind driven polynyas. *J. Geophys. Res.* **92**, 7049–7059.

Rogers, R. R. and Yau, M. K. 1989. *A short course in cloud physics*. Pergamon Press, 3rd edition.

Semtner, A. J. 1976. A model for the thermodynamic growth of sea ice in numerical investigations of climate. *J. Phys. Oceanogr.* **6**, 379–389.

Smith, S. D., Muench, R. D. and Pease, C. H. 1990. Polynyas and leads: an overview of physical processes and environment. *J. Geophys. Res.* **95**, 9461–9479.

Tremblay, L.-B. and Mysak, L. A. 1997. Modelling sea ice as a granular material, including dilatancy effect. *J. Phys. Oceanogr.* **27**, 2342–2360.

Willmott, A. J., Morales Maqueda, M. A. and Darby, M. S. 1997. A model for the influence of wind and oceanic currents on the size of a steady state latent heat coastal polynya. *J. Phys. Oceanogr.* **27**, 2256–2275.

Winsor, P. and Björk, G. 2000. Polynya activity in the Arctic Ocean from 1958 to 1997. *J. Geophys. Res.* **105**, 8789–8803.

Zillman, J. W. 1972. *A study of some aspect of the radiation heat budget of the southern hemisphere oceans.* Report 26, Bureau of Meteorology, Department of Interior, Camberra, Australia.